Nanoscale

Accepted Manuscript

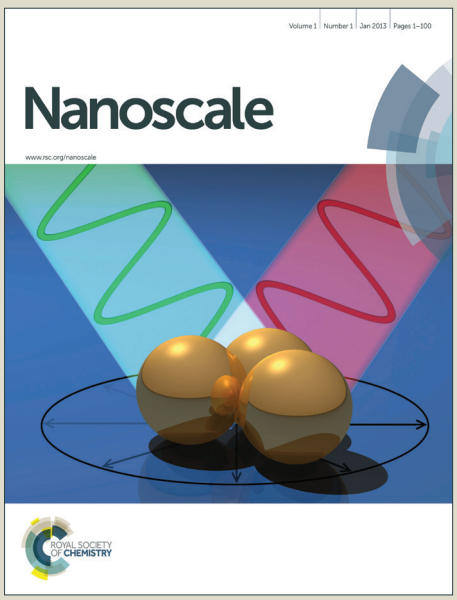

ROYAL SOCIETY OF CHEMISTRY

www.rsc.org/nanoscale

Cite this: DOI: 10.1039/c0xx00000x

www.rsc.org/xxxxxx

PAPER

Bioinspired polyethylene terephthalate nanocone arrays with underwater superoleophobicity and anti-bioadhesion properties

Wendong Liu,[a] Xueyao Liu,[a] Jiaozi Fangteng,[b] Shuli Wang,[a] Liping Fang,[a] Huaizhong Shen,[a] Siyuan Xiang,[a] Hongchen Sun,[b] and Bai Yang*[a]

Received (in XXX, XXX) Xth XXXXXXXXX 20XX, Accepted Xth XXXXXXXXX 20XX
DOI: 10.1039/b000000x

This paper presents a facile method to fabricate bioinspired polyethylene terephthalate (PET) nanocone arrays via colloidal lithography. The aspect ratio (AR) of the nanocones can be finely modulated ranging from 1 to 6 by regulating the etching time. The samples with the AR value of 6 can present underwater superoleophobicity with the underwater oil contact angle (OCA) of 171.8 °. The as-prepared PET nanocone arrays perform anti-bioadhesion behavior which inhibiting the formation of the actin cytoskeleton when it used as the substrate for cell culture. Besides, the oil wettability is temperature controlled after modifying the PET nanocone arrays with PNIPAAm film, and the oil wettability of the functionalized nanocone arrays can be transformed from the superoleophobic state with OCA about 151 ° to the oleophilic state with OCA about 25 °reversibly. Due to the high-throughput, parallel fabrication and cost-efficiency of this method, it will be favourable for researchers to introduce oleophobic properties to various substrate and device surfaces. Attribute to the superoleophobicity and ease functionalizing properties, the PET nanocone arrays are very promising surfaces for anti-adhesion, self-cleaning and having potential applications in material, medical, and biological fields.

1. Introduction

With the highly intersection of chemistry, materials science and bioscience, the cognizing of the nature has been highly developed, a series of bionic structures are fabricated and applied in various fields. [1-3] At the same time, the wettability of the bulk material's surface has aroused great interests of the researchers for its significant impacts on the physicochemical properties, such as adhesion, friction, catalysis and so on. [4-6, 50-51] Researchers begin to aim at learning the surface chemistry and topology of the specific structures that existed in the nature since the superhydrophobic lotus-leaf-inspired structure is successfully fabricated, and a lot of superhydrophobic surfaces with specific wettability are fabricated. [7-8] Although the superhydrophobic structures have great value of applications in the fields like self-cleaning, antifogging and drag reduction, the performance of most superhydrophobic surfaces will decline upon contaminating by oil dirt which is caused by the insufficient oleophobicity. Thus, fabrication of superoleophobic surfaces becomes the most efficient way to solve this issue. And they attracted great research interests for their potential applications in the fields of oil-repellent coatings, anti-crawling materials, marine anti-fouling, fluid power systems, anti-oil treatment of oil pipelines, and anti-bioadhesion. [4, 9-10] Though many works have been published which provides the detailed interpretation of oil wetting behavior, [11-15] it's indeed more difficult to fabricate superoleophobic surfaces with high OCAs than creating superhydrophobic surfaces since most oils possess low surface tension. Up to now, several special microstructures, such as nanofilaments, overhang structures, and re-entrant surface curvatures, have been found to be useful for achieving underwater superoleophobicity. [16] Many underwater superoleophobic surfaces have been obtained based on nanocone clusters, meshes and fish scale inspired structures since Tuteja and coworkers published their work which concentrate on how to design superoleophobic surfaces based on the rough fluorodecyl POSS-PMMA surface which performs superoleophobicity. [3, 17-23] Nevertheless, the fabrication of these structures is always restricted by the specific substrate (usually silicon or metal oxide) and the complicated fabrication processes. [24-28] Recently, several superoleophobic interfaces inspired by fish skin and mussel adhesives have been achieved, providing alternative ideas to prepare superoleophobic surfaces since the micro-nano structures can trap water molecules and repel the oil wetting via forming an solid/water/oil interface. [29-31] Lately, Jiang and co-workers prepared a novel inorganic high-energy coating with underwater low adhesive superoleophobicity inspired by short Clam's shell and Nacre, and then they fabricated a polyelectrolyte/clay hybrid film which enhanced the mechanical property, great abrasion resistance and environment durability in artificial seawater. [52-53] These nature inspired structures have greatly promote the development of the field of fabrication of superoleophobic surfaces and they have great potential use in microfluidic technology and antifouling coating. However, it is still a great challenge to fabricate superoleophobic surfaces on polymer substrate employ low-cost and time-efficient manner.

In the past decade, several methods have been used to fabricate polymer nanostructures, such as electron-beam lithography, scanning probe microscopy lithography, soft lithography and Langmuir–Blodgett lithography. [32] However, they are costly and time-consuming methods to fabricate polymer nanostructures with large area. Moreover, finely controlling the structural parameters, such as shapes and dimensions of the features, is a key point for the polymer nanostructures for applying in the fields of macromolecule sensors, novel micro- or nanofluidic devices and other applications. Therefore colloidal lithography is considered as a comprehensive, low-consumption, and high throughput method for the fabrication of micro- or nanostructures. It possess the following advantages compared with the other methods mentioned above: the colloidal crystals used as masks during the etching process can easily obtained; the structure parameters, such as period, aspect ratio (AR) and so on, can be finely regulated via modulating the diameter of the colloidal particles and the parameters of the etching process; nanostructures with specific symmetry and complex 3D structures can be fabricated as well. According to these advantages, micro- or nanostructures fabricated by colloidal lithography have been widely used in the fields of antireflective, antifogging, sensing and controllable adhesion. [32-35]

These years, micro- and nanocone arrays are of great importance for wide applications in sensing, localized surface plasmon resonance, superhydrophobic and superoleophobic surfaces. [36-37] But cone and cone-like arrays used as superoleophobic surfaces are either mainly based on inorganic materials or with sophisticated fabrication process, [16, 18-19, 38-39] and few works focus on fabricating polymer based nanocone arrays with high aspect ratio. Thus, it is highly significant to develop an efficient method to prepare polymer based nanocone arrays for the antifouling and anti-adhesion studying. In this paper, we report a facile and cost-efficient method to fabricate bioinspired Polyethylene terephthalate (PET) nanocone arrays utilizing colloidal lithography. The AR of the nanocones can be finely modulated ranging from 1 to 6. The samples with the AR value of 6 can present underwater superoleophobicity with the underwater OCA of 171.8 °. The as-prepared PET nanocone arrays perform anti-bioadhesion behavior which inhibiting the formation of the actin cytoskeleton when it used as the substrate for cell culture. Besides, the oil wettability is temperature controlled after modifying the PET nanocone arrays with PNIPAAm film, and the oil wettability of the functionalized nanocone arrays can be transformed between the superoleophobic state (OCA about 151 °) to oleophilic state (OCA about 25 °) reversibly. Due to the high-throughput, parallel fabrication and cost-efficiency of this method, it is will be favorable for researchers to introduce oleophobic properties to various substrate and device surfaces. And attribute to the superoleophobicity and ease functionalizing properties, the PET nanocone arrays are very promising surfaces for anti-adhesion, self-cleaning and having potential applications in material, medical, and biological fields.

2. Experimental Section

2.1. Materials

Polyethylene terephthalate (PET) film with a thickness of 0.2 mm were purchased from AOLIPU and cut into ca. 2.0 cm × 2.0 cm pieces using as substrates, and after sequential ultrasonic cleaning in chloroform ($CHCl_3$) and acetone which were used to remove the impurities that adsorbed on the surface, the PET substrates were rinsed with absolute ethanol for several times and dried with nitrogen gas (N_2) stream. N-isopropyl acrylamide (NIPAAm) monomer was provided by J&K Chemical, phosphate buffer saline was provided by Alfa Aesar. Polystyrene (PS) microsphere with the diameter of 580 nm was synthesized via emulsion polymerization method, [40] 3-Aminopropyltrimethoxysilane (APTMS), 2-bromoisobutyrylbromide, Copper (Ⅰ) chloride (CuCl), tetramethylrhodamine B isothiocyanate (TRITC) labeled phallaoidin, 4, 6-diamidina-2-phenylindole (DAPI), albumin from bovine serum were purchased from Aldrich. N, N, N', N', N"-pentamethyldiethylenetriamine (PMDETA) was purchased from TCI, 4% polyoxymethylene, Triton X-100 was purchased from Beijing DINGGUO Biotechnology. Chloroform, acetone, dichloromethane, 1, 2-dichloroethane, toluene, triethylamine, methanol, absolute ethanol, sodium dodecyl sulfate (SDS) were used as received. The water used in all experiments was deionized and doubly distilled prior to use.

2.2. Fabrication of bioinspired PET nanocone arrays

The PET nanocone arrays were fabricated by a colloidal lithography method. First, the PS microspheres were self assembled on the surface of the cleaned PET substrates to form hexagonal-close-packed (hcp) 2D PS colloidal crystal via the interfacial modification method. [41] In particular, 0.3 mL PS microshere (the diameter is 580 nm) dispersion in the mixture solution of absolute ethanol and deionized water (the volumetric ratio equals 1:1) with a concentration of 0.5% was dropped on the surface of the water in a glass petri dish with the diameter of 15 cm, and then 100 μL SDS solution with the concentration of 3% was added to water surface, and achieving the 2D hcp PS monolayer on the surface of water. After lifting up the monolayer microspheres onto the PET substrate, the 2D colloidal crystals were obtained when the slides dried. Then the PET nanocone arrays were achieved by etching off the PS microsphere experience a non-close-packed state (ncp), meanwhile, etching off the exposed PET substrate by the oxygen reactive ion etching (RIE), which was performed using Plasmalab 80 Plus (Oxford Instrument). During the etching process, the oxygen flow rate performs a major role, while the chamber pressure, RF power and ICP power ensured the stability of the process which determines the time dependence of the feature structure. And if the PS diameter were changed, the oxygen gas flow rate should be preferential regulated while modulating the other parameters to ensure the stability of the new process. Thus, in this work, the RIE operating at 15 mTorr pressure, 20 SCCM oxygen gas flow rate, and RF power of 30 W, ICP power of 30 W was carried out from 5 min to 30 min. After RIE, the retained PS was removed by DMF under ultrasonic bath.

2.3. Functionalizaton of the PET nanocone arrays with PNIPAAm via SI-ATRP

Before the polymerization carried out，the ATRP initiator were grafted onto the surface of PET nanocone arrays by a two-step-reaction method. First, the PET nanocone arrays were

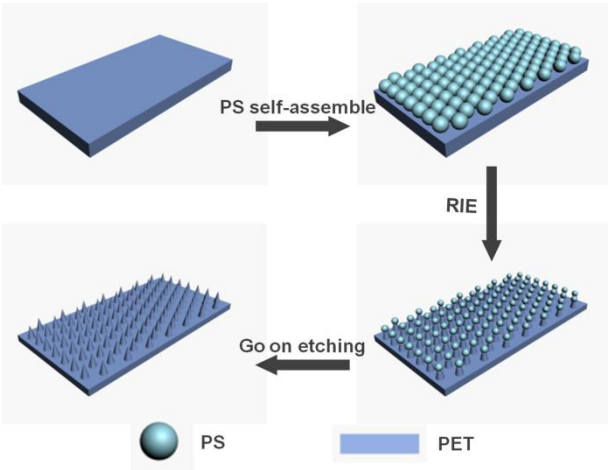

Fig. 1 Typical schematic procedure of fabricating PET nanocone arrays.

hydroxylated under oxygen plasma treatment which was performed using PLASMA CLEANER (HARRICK PLASMA ITHACA, NEW YORK), and then immersed in the mixed solution of 15 mL toluene and 20 μL APTMS for 5 h at room temperature to make the $–NH_2$ graft onto the PET nanocone arrays via the chemical reaction between APTMS and the –OH groups on the PET nanocone arrays. Second, the $–NH_2$ groups modified PET nancone arrays were soaked in the mixed solution of 140 μL triethylamine and 10 mL anhydrous dichloromethane in a sealed vessel, after that 100 μL 2-bromoisobutyrylbromide (the ATRP initiator) was added into the solution containing the $–NH_2$ modified substrates at 0℃, the sealed vessel was left at this temperature for 1h and then placed at room temperature for 15 h. The wafers were rinsed with anhydrous dichoromethane and absolute ethanol for several times, and dried by N_2 stream. For the functionalization of the PET nanocaone arrays, we chose NIPAAm as the monomer to prepare polymer brush on the surface of the substrates by the method of grafting from surfaces. During the polymerization of PNIPAAm, 1.25 g NIPAAm (11.05 mmol) and 140 μL PMDETA (0.67 mmol) were added to 4 mL of an aqueous solution of methanol (the volumetricratio of methanol/H_2O equals 1:1), and the mixtures were shaken in an ultrasonic bath until a homogeneous transparent solution formed. Then the mixture was degassed for 30 min by ultrapure N_2 flow, after that 22 mg (0.22 mmol) CuCl was added into the solution, and it was shaken in an ultrasonic bath until the color of the solution changed into apple green. Lastly, the PET nanocone arrays with initiators were immersed in the solution for 15 min to 60 min under the nitrogen flow at room temperature. After polymerization, the samples were cleaned by absolute ethanol and deionized water for several times and kept at 4 ℃ under a dry atomsphere.

2.4. Cell seeding and staining

In this experiment, the flat PET film and PET nanocone arrays were used as the substrates for cell adhesion. Mouse MC3T3-E1 osteblasts were plated at a density of 1.5×10^5 cells per mL in H-DMEM media were supplemented with 10% fetal bovine serum (FBS) (Gibco) and 1% antibiotics (25.000 $IUmL^{-1}$ penicillin and 25 $mgmL^{-1}$ streptomycin) in 5% CO_2 at 37 ^oC. After culturing for 3 days, the substrates with cell adhered were washed in PBS to remove the physically absorbed organics and prepared to stain.

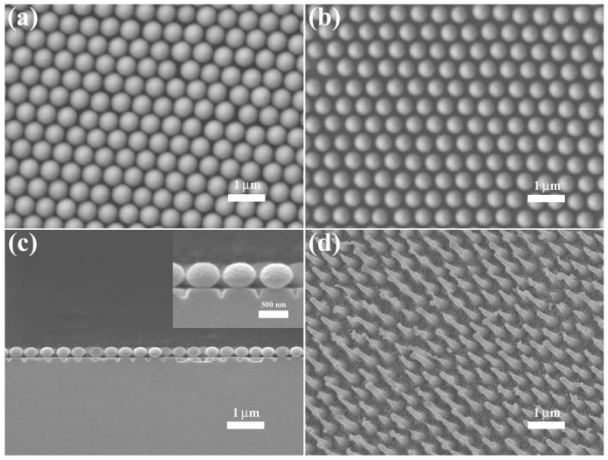

Fig. 2 SEM images of (a) the hexagonal close packed PS microspheres with the diameter of 580 nm, (b) non-close-packed PS microspheres after RIE treatment, (c) cross-section view of the partially etched PET substrate underneath the ncp PS microspheres, inset is the magnified image of the composite structure and (d) tilt view of the PET nanocone arrays with the AR of 6.

For cell immunostaining, the cells were fixed by 4% polyoxymethylene in PBS solution for 20 min and then permeabilized with 0.1% Triton X-100 for 10 min. After that the cells were incubated in a 3% bovine serum albumin blocking agent for 2 h at room temperature and washed twice with PBS buffer. TRITC-phalloidin solution (37.5 $ngmL^{-1}$) were added to the surfaces and incubated for 60 min at room temperature. Cells were thereafter washed three times with PBS and finally incubated with 2 μgmL^{-1} DAPI for 5 min at room temperature and washed three times. Stained cells were kept in PBS at 4 ℃.

2.5. Characterization

SEM images were taken with a JEOL FESEM 6700F electron microscope with primary electron energy of 3 kV. The samples were sputtered with a thin layer of Pt prior to imaging. X-ray photoelectron spectroscopy (XPS) was investigated by using ESCALAB 250 spectrometer with a mono X-Ray source Al Ka excitation (1486.6 eV). The oil (1, 2-dichloroethane) contact angles under water were measured using Dataphysics OCA20. An oil droplet of 3 μL was dropped onto the samples that immersed in water and static contact angle (CA) was determined by the average of at least five measurements taken at different positions on each sample used as the indicator to evaluate the wetting property of the nanocone arrays. The water CA was measured with a water droplet of 3 μL was dropped onto the samples in the air. The optical microscope images and confocal fluorescent microscopy images of the cell cultured on the flat PET film and PET nanocone arrays were taken by the microscopy OLYMPUS BX51 and laser scanning confocal microscopy OLYMPUS BX81 (FluoView^{TM} FV1000) respectively.

3. Results and Discussions

3.1. Fabrication and modulation of the PET nanocone arrays via colloidal lithography

The PET nanocone arrays are fabricated by a colloidal lithography method. Fig. 1 shows the schematic illustration of this process. Firstly, the two-dimensional (2D) hexagonal-close-

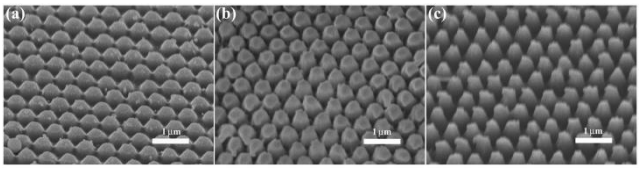

Fig. 3 Tilt view SEM images of the (a) joint state, (b) transition state and (c) completely isolated state of the PET nanocone arrays presented after etching for 4 min, 6 min and 8 min, respectively.

packed (hcp) colloidal crystal was assembled on the surface of the cleaned polyethylene terephthalate (PET) substrate by the interfacial modification method as described in the experimental section. Secondly, the 2D colloidal crystals on the PET substrates were used as the mask, and etching off the exposed PET substrate during the reactive ion etching (RIE) treatment, after the hcp 2D colloidal crystals changed into a ncp one, the etching process went on until the PS microsphere were etched off completely, then the PET nanocone arrays were obtained.

To evaluate the process of the nanocone arrays formation, samples of the different stages during the etching process were characterized by SEM. Fig. 2a presents the hcp structure of the PS mask, the area of the finely arranged hcp PS microsphere can reach 100 μm^2. Fig. S1 shows the optical microscopy image of the self assembled PS microsphere lifted up to the substrate of 4 cm^2, which contains some line and point defects while the PS microsphere occupied more than 99% of the area, and this ensured the quality of the PET nanocone arrays achieved later. After the PS microsphere partially etching off, the colloidal layer formed an ncp structure (Fig. 2b) which maintained the order of the hcp one, meanwhile the PET substrate underneath the PS microsphere were etched off simultaneously when the areas between the spheres were exposed to the oxygen plasma as the PS turn small (Fig. 2c), and this result provides the chance to achieve the well ordered PET nanocone arrays (Fig. 2d) which maintain the order of the PS mask and have a high AR of 6. Taking the advantage of the PS monolayer, PET nanocone arrays with a large area can be obtained while possess some point and line defects (Fig. S2).

Since the formation of the PET based structure was greatly dependent on the etching process, we regulated the etching time of the RIE process to make it clear how the nanocone was formed during the colloidal lithography. Fig. 3 presents the SEM images of the PET structures achieved with the etching time of 4 min (Fig. 3a), 6 min (Fig. 3b) and 8 min (Fig. 3c) respectively. Significantly, three specific states of the PET nanoarrays, named joint state, transition state, completely isolated state were achieved. With increasing the etching time, the diameter of the PET structures decreases and the distances between the nanostructures become larger. For the sample being etched for 4 min, the spaces between two ncp microspheres are so small which resulted in a partially etching in the exposed area, thus the PET nanoarrays present a joint state and have a dome morphology (Fig. 3a). When increasing the etching time to 6 min, the diameter of the PS further reduced, which gave more chance for the exposed PET substrate to react with oxygen plasma. Though it is still not enough to form a completely isolated state, the height of the nanostructure went on and the nanocone arrays preliminarily shows the cone morphology, and the PET nanoarrays performs an exhibit trend of isolated state which we called it transition state (Fig. 3b). When the etching time reaches 8 min, the top of each structure performs cone morphology and the distances between the nanoarrays were large enough to show completely isolated morphology (Fig. 3c). These results proved that the PET nanocone arrays with a high AR had been successfully fabricated and the morphology could be regulated via tuning the etching time. We provide a facile method to fabricate polymer based nanocone arrays and this method can broaden the use of other function polymers.

3.2. Underwater superoleophobic surfaces formed by PET nanocone arrays

As we know that the wettability properties of nanoarrays are greatly depended on the aspect ratio, thus it is meaningful to modulate the AR via tuning the parameters during the fabrication process.

In this experiment, the feature structure of the PET nanocone arrays can be finely controlled by regulating the experimental conditions. For the samples with same period, the AR of the PET nanocones can be precisely modulated by the etching time of the RIE process.

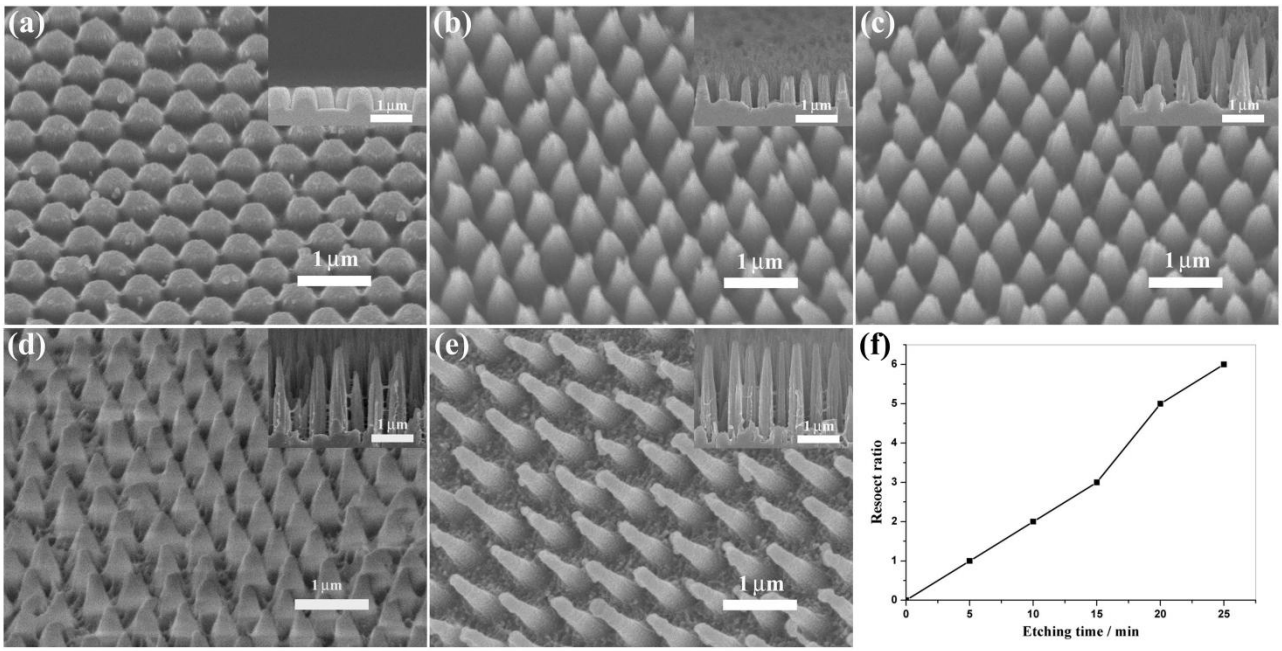

Fig. 4 Tilt view SEM images of the PET nanocone arrays with AR of 1 (a), 2 (b), 3 (c), 5 (d) and 6 (e), respectively. The insets are the corresponding cross-section view. (f) The feature AR revolution of the PET nanocone arrays with the etching time.

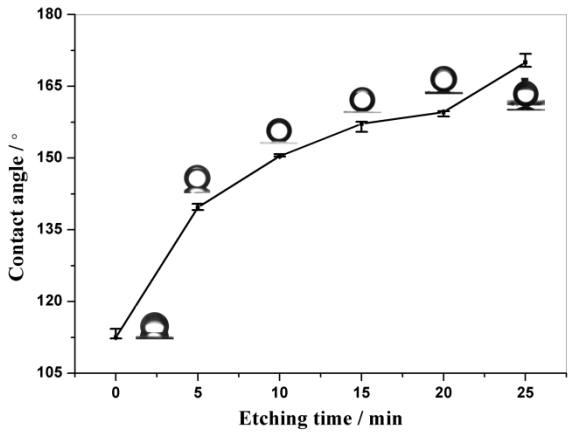

Fig. 5 Underwater OCA as a function of the etching time applied during the fabrication of PET nanocone arrays.

Fig. 4a-e shows the tilt view SEM images of the PET nanocone arrays with the same period but different aspect ratios, the different aspect ratios result from the different etching time are used during the process of fabricating the PET nanocone arrays. The etching time was 5 min (Fig. 4a), 10 min (Fig. 4b), 15 min (Fig. 4c), 20 min (Fig. 4d) and 25 min (Fig. 4e) respectively. From the SEM images we can get the information that the distances between nanocones and the height of the nanostructure raised with the etching time increases during the RIE process. And then the AR of the nanocones in each image was measured according to the cross-view SEM image of each inset, the results show that the major AR is 1 (Fig. 4a), 2 (Fig. 4b), 3 (Fig. 4c), 5 (Fig. 4d) and 6 (Fig. 4e) respectively. The feature AR revolution of the PET nanocone arrays with the etching time was shown in Fig. 4f. These results demonstrate that we can continuously regulate the AR of the nanocone structure via choosing the appropriate etching time of the RIE step. But if the etching time in this experiment increased to 30 min, the PET nanocone arrays have a higher aspect ratio, meanwhile, the nanocone arrays cannot preserve perpendicular to the matrix and aggregated into a cluster state as shown in Fig. S3, it seems that the diameter of the nanocone is so small that the strength of PET cannot keep in a vertical state when in such a high AR, and the flow of oxygen plasma also accelerate the formation of the cluster state. However, this clustered state could not be reproduced. Thus 25 min etching is the best condition to fabricate PET nanocone arrays with the highest AR of 6 in this system.

To evaluate the wettability of the PET nanocone arrays with different aspect ratios, static underwater CAs were measured. An oil (1, 2-dichloroethane) droplet of 3 μL was dropped onto the sample that immersed in water and static CA was determined by the average of the CA which were measured at least five times and taken at different positions on each sample, and static CA was used as an indicator to evaluate the wetting property of the nanocone arrays. Fig. 5 shows the underwater OCA as a function of the etching time applied during the fabrication of the PET nanocone arrays. The chart shows that the underwater OCA presents an increasing trend with prolonging the etching time. When the etching time is longer than 10 min meanwhile the AR is higher than 2, the PET nanocone arrays perform underwater superoleophobic property with the OCA over 150 °. These results following the *Cassie Theory*, [42] there formed a water interlayer which filled the spaces between the nanocones since the PET nanocone itself has certain hydrophilicity (Fig. S4) allowing the water wetting, and the water interlayer greatly hindered the oil wetting, making the surface shows oleophobicity. The PET nanocone arrays transformed into an underwater superoleophobic surface when the AR reaches a critical value. It's worth mentioning that the oil CA can reach 171.8 ° as the AR of the PET nanocone arrays is 6, which is the maximum of this system can reach. Thus the PET nanocone arrays with the AR of 6 were

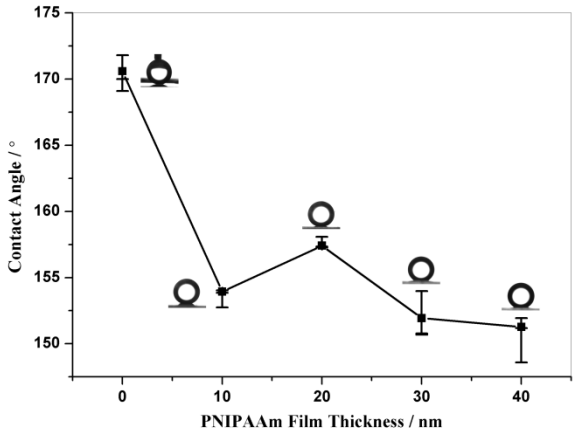

Fig. 6 Underwater OCA as a function of the thickness of PNIPAAm film grafted on PET nanocone arrays.

chosen to do other researches in the following.

These results indicate that the PET nanocone arrays of different AR with the maximum of 6 can be fabricated via reasonable design and operation, meanwhile the wettability of the nanocone arrays can be easily modulated to underwater superoleophobic state with the maximum oil CA of 171.8 °, and it provides the foundation for the structured surface which own the flexibility to be applied in the fields of anti-oil-fouling, self-cleaning and introducing oleophobic properties to various substrate and device surfaces.

3.3. Temperature controlled oil wettability of the functionalized PET nanocone arrays

For the purpose of fabricating a surface with the feature of wettability switching, the functionalized PET nanocone arrays were prepared via grafting poly (N-isopropyl acrylamide) (PNIPAAm) to the nanocone arrays' surface by the surface-initiated atom-transfer-radical polymerization (SI-ATRP) method. [32] The schematic illustration of the nanocone arrays modification was shown in Fig. S5. For the purpose of grafting PNIPAAm onto the nanocone surface, the PET nanocone arrays with the AR of 6 were treated with oxygen plasma to make their surfaces hydrophilic and then grafted the ATRP initiator to the surface via the two-step method mentioned in the experimental section. After the initiator grafting, different thickness of PNIPAAm modified PET nanocone arrays were obtained through regulating the polymerization time from 15 to 60 min, the thickness of the PNIPAAm films was 10 nm, 20 nm, 30 nm, and 40 nm respectively. Fig. S6 presents the XPS spectra of the PNIPAAm modified PET nanocone arrays, the proportion of oxygen and nitrogen is about 1.5 which proved that the PNIPAAm were succussully grafted onto the PET nanocone arrays since the nitrogen are mainly contained in the polymer chains but not contained in the PET nanocone arrays. Then the oil CA measurements were carried out to characterize the wettability of the functionalized nanocone arrays. Fig. 6 presents the underwater OCA as a function of the thickness of PNIPAAm film grafted on the PET nanocone arrays. From the chart, we can get the information that when PET nanocone arrays which possess superoleophobicity grafted with a thin film of PNIPAAm, the OCA showed an obvious decrease with the value below 150 °.

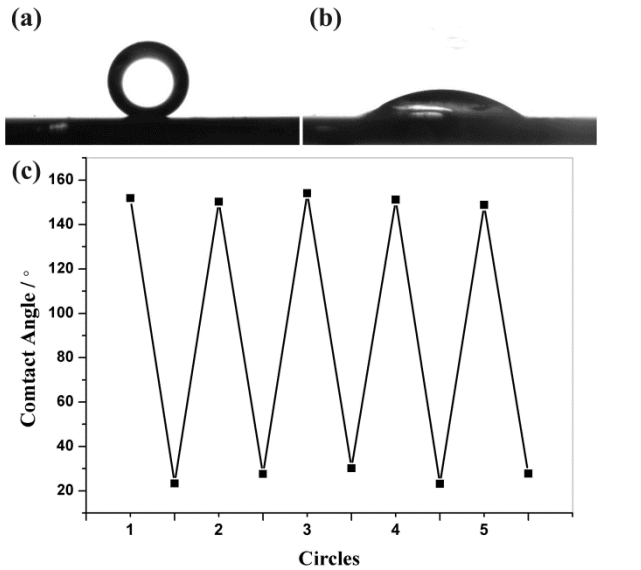

Fig. 7 Underwater OCA obtained at 20 ℃ (a) and 60 ℃ (b), (c) the reversible underwater OCA transition of the PNIPAAm functionalized PET nanocone arrays at 20 ℃ (below the LCST of PMIPAAm) and 60 ℃ (above the LCST of the PNIPAAm).

When the thickness of PNIPAAm increased to 20 nm, the surface return to the superoleophobic state with the OCA above 150 °; Keeping increasing the thickness of PNIPAAm film to 30 and 40 nm, the OCA decrease again with lower values than the one with a thickness of 10 nm. Hence, there is an appropriate modified thickness of the specific structure to keep the superoleophobicity, and 20 nm was chosen as the ideal thickness of the PNIPAAm film to modify the PET nanocone arrays with the highest aspect ratio. In order to verify the oil wettability transition with the temperature variation, the underwater OCA measurement was conducted. The underwater OCA decrease from 151.89 ° to 23.32 °when the temperature increase from 20 ℃ to 60 ℃, and the wetting behavior returns to the original state upon cooling, indicating a reversible switch between wetting states of superoleophobicity and oleophilicity. Fig. 7 shows the optical images of the oil droplet on the PNIPAAm modified PET nanocone arrays obtained at 20 ℃ (Fig. 7a) and 60 ℃ (Fig. 7b). The reversible underwater OCA transition of the PNIPAAm functionalized PET nanocone arrays at different temperatures (20 ℃, below the lower critical solution temperature (LCST) of PNIPAAm, and 60 ℃, above the LCST of PNIPAA) was shown in Fig. 7c, indicating the excellent reproducibility and stability of the wettability transition. The wettability switching attributed to the phase transformation of PNIPAAm with the temperature reciprocating transform from below the LCST to above the LCST [12]. When the temperature is below LCST, intermolecular hydrogen bonds with water, leading to a hydrated, swollen state of PNIPAAm which exhibits hydrophilicity and keeps the wetting behavior following the *Cassie*-like state. [42] When the temperature increases to above LCST, the PNIPAAm film performs a shrink state which exposes the hydrophobic groups to the outside and presents hydrophobicity, thus causing the wetting behavior transition from *Cassie*-like state to *Wenzel*-like state [43] which resulting in the decrease of OCA with the value drop to about 23 °. Based on this wetting behavior transition model, the

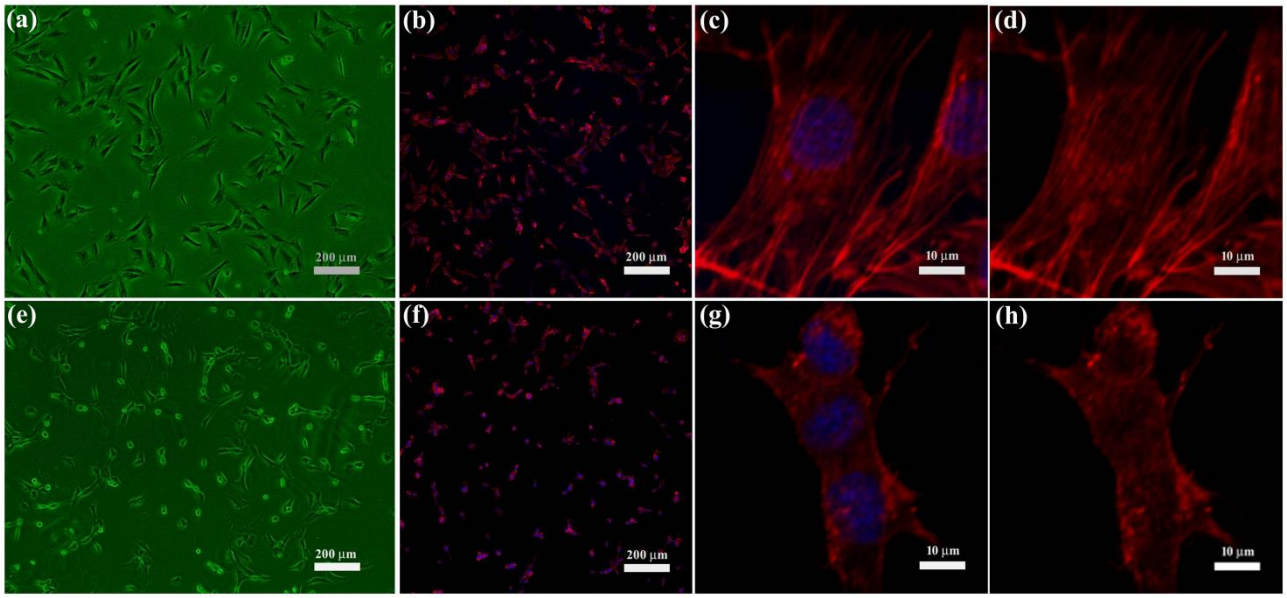

Fig. 8 Optical microscopy images (a, e) and confocal fluorescent microscopy images (b-d, f-h) of the cell cultured on the flat PET film (a-d) and PET nanocone arrays (e-h): blue-the nucleus; red-the actin cytoskeleton.

reversible underwater OCA transition of the PNIPAAm functionalized PET nanocone arrays carried out with temperature changes. These results prove that after the PET nanocone arrays are functionalized with PNIPAAm, the oil wettability of the nanocone arrays can be transformed freely between the superoleophobic state (OCA about 151 °) and the oleophilic state (OCA about 23 °). Hence, the functionalized PET nanocone arrays endowed this specific nanostructure great potential application in controllable separation of water and oil mixtures, filtration and microreactors, lab-on-chip devices and so on.

3.4. Inhibition of cell adhesion performed on the PET nanocone arrays.

The PET nanocone arrays had a great effect on anti-adhesion since it possesses the underwater superoleophobicity. The PET nanocone arrays with the AR of 6 were used as the substrate for cell culture, meanwhile the flat PET films were used as negative control. After culturing for 3 days, the actin cytoskeleton and cell nucleus were stained with TRITC-phalloidin and DAPI respectively. Fig. 8 showed the optical microscopy images (Fig. 8a, 8e) and confocal fluorescent microscopy images (Fig. 8b-d, Fig. 8f-h) of the cell cultured on the flat PET film (Fig. 8a-d) and PET nanocone arrays (Fig. 8e-h) with the stained color of blue and red representing the nucleus and the actin cytoskeleton respectively. The images confirm that mouse MC3T3-E1 osteblasts adhered well onto the flat PET substrate and the cells maintained good biological activity since the cells performed great degree of spreading （Fig. 8a-b）. However, the adhesion behaviors are different on the substrates with nanocone arrays for that most of the cells perform a circle-like or short rod-like shape but not the highly spread morphology (Fig. 8e-f), indicating that the cell adhesion was inhibited on the PET nanocone arrays. To make it clear that whether the PET nanocone arrays have a negative influence on cell adhesion, the magnified images of the stained actin cytoskeleton of the cells on both substrates were obtained with the help of laser scanning confocal microscopy. Fig. 8c, 8g showed the merged images of stained nucleus and cytoskeleton of the cells cultured on the flat PET film and PET nanocone arrays respectively. The nucleus staining images show that the nucleus maintained ellipse or round morphology without splitting which proved that the cells maintained good biological activity on both substrates before staining. Besides, the cells adhered to the flat PET film performed spread morphology (Fig. 8b) while the rigid actin cytoskeleton which throughout the spread cells from one side to the other side (Fig. 8d) forming. The cells adhered to the nanocone arrays performed disc and short rod-like morphology (Fig. 8f) and actin showed a disordered aggregating state with no rigid cytoskeleton forming which indicated that the cell adhesion were greatly inhibited, consistent with the results of other researchers. [44-49] The anti-bioadhesion property of the PET nanocone arrays resulted from the superoleophobicity which weakened the interactions between the substrate and adhesion proteins secreted by the cells, and thus decreased the strength of stress which acts on the cell anchored to the substrate. In such a case, the formation of actin cytoskeleton was inhibited, which resulted in an anti-bioadhesion effect. These results proved that the underwater superoleophobicity of the underlying structure had a great effect on anti cell adhesion and the formation of the actin cytoskeleton. Further experiments are needed to be done for us to draw more specific conclusions. Besides, the anti-adhesion property of the PET nanocone arrays could widen the applications of this bioinspired artificial structure in materials, medical, and biological fields.

4. Conclusion

In summary, a novel facile method to fabricate bioinspired nanocone arrays with the high aspect ratio, which can be used as underwater superoleophobic surface is presented. By using this method, PET nanocone arrays with different aspect ratios and

feature oil wettabilities can be prepared over a large area, and the highest AR of the nanocone arrays can reach 6, and presents underwater superoleophobicity with the underwater OCA equals 171.8 °. The as-prepared PET nanocone arrays perform anti-bioadhesion behavior which inhibiting the formation of the actin cytoskeleton. Besides, the oil wettability can be temperature controlled after the PET nanocone arrays functionalized with PNIPAAm film and the oil wettability of the modified nanocone arrays can be transformed between the superoleophobic state (OCA about 151 °) and the oleophilic state (OCA about 25 °) reversibly. As a result, the PET nanocone arrays are very promising surfaces for anti-adhesion, anti-oil-fouling, self-cleaning. Due to the high-throughput, parallel fabrication and cost-efficiency of this method, it will be favourable for researchers to introduce oleophobic properties to various substrate and device surfaces. And attribute to the superoleophobicity and ease functionaling properties, the PET nanocone arrays are very promising surfaces for anti-adhesion, self-cleaning and having potential applications in material, medical, and biological fields.

Acknowledgment

This work was financially supported by the National Basic Research Program of China (973 program) under Grant No. 2012CB933800, and the National Science Foundation of China (NSFC) under Grand Nos. 91123031, 21221063, 51373065.

Notes and references

[a] *State Key Laboratory of Supramolecular Structure and Materials, College of Chemistry, Jilin University, Changchun 130012, People's Republic of China. Fax: +86 431 85193423; Tel: +86 431 85168478; E-mail: byangchem@jlu.edu.cn.*

[b] *School of Stomatology, Jilin University, Changchun 130041, People's Republic of China.*

† Electronic Supplementary Information (ESI) available: The optical microscopy image of the self assembled 2D PS microspheres over a large area, the diameter of the PS microsphere is 580 nm; The top-view SEM image of the PET nanocone arrays over a large area, the AR of the nanocone is 6; The SEM image of the PET nanocone arrays obtained after 30 min etching; The optical image of the water droplet on the PET nanocone arrays with the AR of 6; The schematic illustration of the nanocone arrays modification with PNIPAAm; High resolution XPS spectra of the PNIPAAm modified PET nanocone arrays. See DOI: 10.1039/b000000x/

1 P.-Y. Chen, J. McKittrick and M. A. Meyers, *Prog. Mater Sci.*, 2012, **57**, 1492.
2 T. Sun, G. Qing, B. Su and L. Jiang, *Chem. Soc. Rev*., 2011, **40**, 2909.
3 M. Liu, S. Wang, Z. Wei, Y. Song and L. Jiang, *Adv. Mater*. 2009, **21**, 665.
4 N. Valipour M, F. C. Birjandi and J. Sargolzaei, *Colloid. Surface. A*, 2014, **448**, 93.
5 E. Ueda and P. A. Levkin, *Adv. Mater*. 2013, **25**, 1234.
6 S. Pan, A. K. Kota, J. M. Mabry and A. Tuteja, *J. Am. Chem. Soc.*, 2013, **135**, 578.
7 T. Darmanin and F. Guittard, *Prog. Polym. Sci.*, 2014, **39**, 656.
8 Z. Chu and S. Seeger, Chem. *Soc. Rev.*, 2014, **43**, 2784.
9 E. Ueda and P. A. Levkin, *Adv. Mater.*, 2013, **25**, 1234.
10 S. Pan, A. K. Kota, J. M. Mabry and A. Tuteja, *J. Am. Chem. Soc.*, 2013, **135**, 578.
11 H. Bellanger, T. Darmanin, E. Taffin de Givenchy and F. Guittard, *Chem. Rev.*, 2014, **114**, 2694.
12 B. Xue, L. Gao, Y. Hou, Z. Liu and L. Jiang, *Adv. Mater*., 2013, **25**, 273.
13 V. Hejazi, A. E. Nyong, P. K. Rohatgi and M. Nosonovsky, *Adv. Mater*., 2012, **24**, 5963.
14 T. Neckernuss, S. Wiedemann, A. Plettl and P. Ziemann, *Adv. Mater. Interfaces*, 2014, DOI: 10.1002/admi.201300033.
15 K. H. Chu, R. Xiao and E. N. Wang, *Nat. Mater*., 2010, **9**, 413.
16 W. Ma, H. Xu and A. Takahara, *Adv. Mater. Interfaces*, 2014, DOI: 10.1002/admi.201300092.
17 A. Tuteja, W. Choi, M. Ma, J. M. Mabry, S. A. Mazzella, G. C. Rutledge, G. H. McKinley and R. E. Cohen, *Science*, 2007, **318**, 1618.
18 J. Zhang and S. Seeger, *Adv. Funct. Mater*., 2011, **21**, 4699.
19 J. Zhang and S. Seeger, *Angew. Chem. Int. Ed*., 2011, **50**, 6652.
20 X. Yao, J. Gao, Y. Song and L. Jiang, *Adv. Funct. Mater*., 2011, **21**, 4270.
21 S. Pechook, N. Kornblum and B. Pokroy, *Adv. Funct. Mater*., 2013, **23**, 4572.
22 Z. Xue, S. Wang, L. Lin, L. Chen, M. Liu, L. Feng and L. Jiang, *Adv. Mater*., 2011, **23**, 4270.
23 L. Zhang, Y. Zhong, D. Cha and P. Wang, *Sci. Rep*., 2013, **3**, 2326.
24 L. P. Xu, J. Zhao, B. Su, X. Liu, J. Peng, Y. Liu, H. Liu, G. Yang, L. Jiang, Y. Wen, X. Zhang and S. Wang, *Adv. Mater*., 2013, **25**, 606-611.
25 S. Zhang, F. Lu, L. Tao, N. Liu, C. Gao, L. Feng and Y. Wei, *ACS Appl. Mater. Interfaces*, 2013, **5**, 11971.
26 J. Yang, Z. Zhang, X. Xu, X. Zhu, X. Men and X. Zhou, *J. Mater. Chem*. 2012, **22**, 2834.
27 Y. Dong, J. Li, L. Shi, X. Wang, Z. Guo and W. Liu, *Chem. Commun.*, 2014, **50**, 5586.
28 L. Cao and D. Gao, *Faraday Discuss*., 2010, **146**, 57.
29 H. Lee, S. M. Dellatore, W. M. Miller and P. B. Messersmith, *Science*, 2007, **318**, 426.
30 Y. Cai, L. Lin, Z. Xue, M. Liu, S. Wang and L. Jiang, *Adv. Funct. Mater*., 2014, **24**, 809.
31 K. Liu, Y. Tian and L. Jiang, *Prog. Mater Sci*., 2013, **58**, 503.
32 W. Liu, Y. Li, T. Wang, D. Li, L. Fang, S. Zhu, H. Shen, J. Zhang, H. Sun and B. Yang, *ACS Appl. Mater. Interfaces*, 2013, **5**, 12587.
33 J. Zhang, Y. Li, X. Zhang, and B. Yang, *Adv. Mater*., 2010, **22**, 4249.
34 W. Liu, Y. Li and B. Yang, *Sci. China Chem*., 2013, **56**, 1087-1100.
35 Y. Li, J. Zhang and B. Yang, *Nano Today*, 2010, **5**, 117.
36 K. Seo, M. Wober, P. Steinvurzel, E. Schonbrun, Y. Dan, T. Ellenbogen and K. B. Crozier, *Nano Lett*., 2011, **11**, 1851.
37 Y. Dong, J. Li, L. Shi, X. Wang, Z. Guo and W. Liu, *Chem. Commun*., 2014, **50**, 5586.
38 H.-B. Jo, J. Choi, K.-J. Byeon, H.-J. Choi and H. Lee, *Microelectron. Eng*., 2014, **116**, 51.
39 J.-Y. Shiu, C.-W. Kuo, P. Chen and C.-Y. Mou, *Chem. Mater*., 2004, **16**, 561.
40 J. Zhang, Z. Chen, Z. Wang, W. Zhang and N. Ming, *Mater. Lett*., 2003, **57**, 4466.
41 Y. Li, J. Zhang, S. Zhu, H. Dong, F. Jia, Z. Wang, Z. Sun, L. Zhang, Y. Li, H. Li, W. Xu and B. Yang, *Adv. Mater*., 2009, **21**, 4731.
42 A. B. D. B. Cassie, S., *Trans. Faraday Soc*., 1944, **40**, 546.
43 R. N. Wenzel, *Ind. Eng. Chem*., 1936, **28**, 988.
44 M. Thery, V. Racine, M. Piel, A. Pepin, A. Dimitrov, Y. Chen, J. B. Sibarita and M. Bornens, *Proc. Natl. Acad. Sci. U. S. A*., 2006, **103**, 19771.
45 C. Y. Tay, S. A. Irvine, F. Y. Boey, L. P. Tan and S. Venkatraman, *Small*, 2011, **7**, 1361.
46 M. Thery, V. Racine, A. Pepin, M. Piel, Y. Chen, J. B. Sibarita and M. Bornens, *Nat. Cell Biol*., 2005, **7**, 947.
47 W. Ronan, V. S. Deshpande, R. M. McMeeking and J. P. McGarry, *Biomech. Model. Mechan*., 2014, **13**, 417.
48 X. Xiao, D. D. Mruk, E. I. Tang, C. K. Wong, W. M. Lee, C. M. John, P. J. Turek, B. Silvestrini and C. Y. Cheng, *Hum. Reprod*., 2014, **29**, 1279.
49 S. Yamashiro, H. Mizuno, M. B. Smith, G. L. Ryan, T. Kiuchi, D. Vavylonis and N. Watanabe, *Mol. Biol. Cell*, 2014, **25**, 1010.

50 X. Tang, Y. Si, J. Ge, B. Ding, L. Liu, G. Zheng, W. Luo and J. Yu, *Nanoscale*, 2013, **5**, 11657.
51 Y. Wu, T. Hang, J. Komadina, H. Ling and M. Li, *Nanoscale*, 2014, **6**, 9720.
52 X. Liu, J. Zhou, Z. Xue, J. Gao, J. Meng, S. Wang and L. Jiang, *Adv. Mater.*, 2012, **24**, 3401.
53 L. Xu, J. Peng, Y. Liu, Y. Wen, X. Zhang, L. Jiang and S. Wang, *ACS Nano*, 2013, **7**, 5077.